Dynamics of a large, restless, rhyolitic magma system at Laguna del Maule, southern Andes, Chile

Brad S. Singer*, Nathan L. Andersen, Hélène Le Mével, Kurt L. Feigl, Charles DeMets, Basil Tikoff, Clifford H. Thurber, Brian R. Jicha, *University of Wisconsin–Madison, Dept. of Geoscience, Madison, Wisconsin 53706, USA;* ***Carlos Cardona,*** *Observatorio Volcanológico de los Andes del Sur (OVDAS) and SERNAGEOMIN, Chile, and Universidad de Concepción, Chile;* ***Loreto Córdova, Fernando Gil,*** *Observatorio Volcanológico de los Andes del Sur (OVDAS) and SERNAGEOMIN, Chile;* ***Martyn J. Unsworth,*** *University of Alberta, Dept. of Physics, 116 Street and 85 Ave., Edmonton, Alberta T6G 2R3, Canada;* ***Glyn Williams-Jones, Craig Miller,*** *Dept. of Earth Sciences, Simon Fraser University, 8888 University Drive, Burnaby, British Columbia V5A 1S6, Canada;* ***Judy Fierstein, Wes Hildreth,*** *and* ***Jorge Vazquez,*** *U.S. Geological Survey, 345 Middlefield Road, MS 977, Menlo Park, California 94025, USA*

ABSTRACT

Explosive eruptions of large-volume rhyolitic magma systems are common in the geologic record and pose a major potential threat to society. Unlike other natural hazards, such as earthquakes and tsunamis, a large rhyolitic volcano may provide warning signs long before a caldera-forming eruption occurs. Yet, these signs—and what they imply about magma-crust dynamics—are not well known. This is because we have learned how these systems form, grow, and erupt mainly from the study of ash flow tuffs deposited tens to hundreds of thousands of years ago or more, or from the geophysical imaging of the unerupted portions of the reservoirs beneath the associated calderas. The Laguna del Maule Volcanic Field, Chile, includes an unusually large and recent concentration of silicic eruptions. Since 2007, the crust there has been inflating at an astonishing rate of at least 25 cm/yr. This unique opportunity to investigate the dynamics of a large rhyolitic system while magma migration, reservoir growth, and crustal deformation are actively under way is stimulating a new international collaboration. Findings thus far lead to the hypothesis that the silicic vents have tapped an extensive layer of crystal-poor, rhyolitic melt that began to form atop a magmatic mush zone that was established by ca. 20 ka with a renewed phase of rhyolite eruptions during the Holocene. Modeling of surface deformation, magnetotelluric data, and gravity changes suggest that magma is currently intruding at a depth of ~5 km. The next phase of this investigation seeks to enlarge the sets of geophysical and geochemical data and to use these observations in numerical models of system dynamics.

INTRODUCTION

Caldera-scale rhyolitic volcanoes can rapidly deposit hundreds of cubic kilometers of ash over several million square kilometers, threatening people and agriculture at the scale of an entire continent (Sparks et al., 2005; Lowenstern et al., 2006; Self, 2006). Sooner or later, Earth will experience another eruption of this magnitude (Lowenstern et al., 2006; Self and Blake, 2008); consequently, there is a need to gather comprehensive information and create multi-scale models that realistically capture the dynamics leading to these destructive events. Most of our current understanding of this type of volcanic system has been gleaned from the study of eruptive products long after the catastrophic eruption, including voluminous ash flow deposits, such as the Bishop, Bandelier, Huckleberry Ridge, and Oruanui Tuffs (Lowenstern et al., 2006; Hildreth and Wilson, 2007; Bachmann and Bergantz, 2008; Wilson, 2008). The most recent rhyolitic "super-eruption" produced the Oruanui Tuff 26,500 years ago in New Zealand. Even in this relatively recent case, the geologic evidence has been partly obliterated by caldera-collapse, erosion, and burial (Wilson et al., 2005). Moreover, probing the present-day structures beneath a number of calderas using seismic tomography (e.g., Romero et al., 1993; Steck et al., 1998; Farrell et al., 2014) or other geophysical measures (e.g., Lowenstern et al., 2006; Battaglia et al., 2003; Tizzani et al., 2009) has not detected eruptible domains of crystal-poor melt in the shallow crust, nor has it captured the dynamics that preceded these large eruptions.

This paper focuses on the Laguna del Maule Volcanic Field, Chile, a large, potentially hazardous, rhyolitic magmatic system, where an alarming rate of surface uplift for the past seven years and concentrated swarms of shallow earthquakes prompted Observatorio Volcanológico de los Andes del Sur (OVDAS) to declare in March 2013 a yellow alert, signaling a potential eruption within months or years. Straddling the Andean range crest at 36° S (Fig. 1A), this volcanic field features: (1) 13 km^3 of rhyolite that erupted both explosively and effusively during the past 20 k.y.; (2) a zone of low electrical resistivity in the shallow crust below the deforming area; (3) widespread elevated CO_2 concentrations; and (4) a negative (~10 mGal) Bouguer anomaly and preliminary evidence for a positive dynamic gravity signal indicating mass addition.

The underlying magma system has been sampled by eruptions numerous times since its apparent inception in the late Pleistocene, including a dozen crystal-poor, glassy rhyolitic lavas during the Holocene. Linking the assembly and evolution of this

GSA Today, v. 24, no. 12, doi: 10.1130/GSATG216A.1.

*E-mail: bsinger@geology.wisc.edu

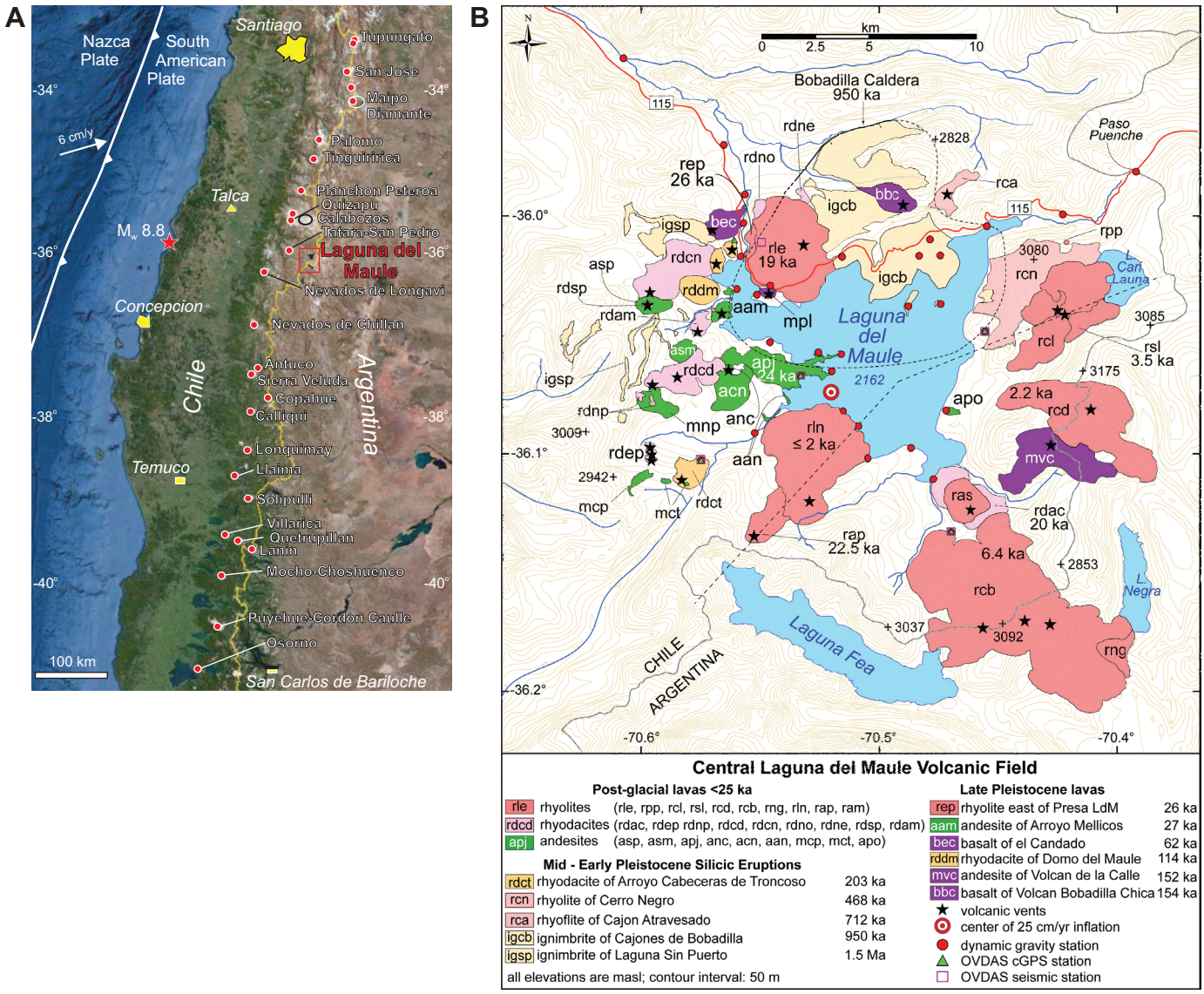

Figure 1. (A) Location of Laguna del Maule volcanic field. Andean Southern Volcanic Zone frontal arc volcanoes are red circles. Red star denotes epicenter of M_W 8.8 earthquake of 27 Feb. 2010 (base from Google Earth). (B) Simplified map of Laguna del Maule volcanic field adapted from Hildreth et al. (2010). Ages of lava flows determined by $^{40}Ar/^{39}Ar$ dating given in k.y.; many of these dates have been determined or revised recently (Andersen et al., 2013). The dam (la presa) at the northern outlet of the lake serves as a useful geographic reference.

large, youthful system on geologic time scales to magma-crust interactions over human time scales while it is actively growing is an exciting frontier for multidisciplinary research. Here we present initial findings, although the ultimate goal is to use these, together with seismic and other data yet to be acquired, in novel ways to create and test a unified computational model of how these hazardous systems operate.

THE LAGUNA DEL MAULE VOLCANIC FIELD

Geology, Geochronology, Geochemistry

The Laguna del Maule volcanic field is 230 km east of the epicenter of the M_W 8.8 Maule earthquake of 27 February 2010, atop one of the most seismically and volcanically active subduction zones on Earth (Fig. 1A). Geologic mapping and $^{40}Ar/^{39}Ar$ geochronology reveal that 350 km^3 of lavas and tuffs of basaltic to rhyolitic composition erupted during the Pleistocene (Hildreth et al., 2010). Previous large-volume explosive silicic eruptions are recorded by a 1.5 Ma dacitic ignimbrite and a 950 ka rhyodacitic tuff associated with the Bobadilla caldera (Fig. 1B). Activity culminated in a spectacular concentric ring of 36 separate post-glacial silicic eruptions between 25 ka and perhaps as recently as 2 ka or later. These most recent eruptions were from 24 vents and produced 15 rhyodacite and 21 rhyolite coulées and lava domes. The vents encircle the 23.5 × 16.5 km lake basin, with the 36 silicic flows comprising 6.4 km^3 of mainly phenocryst-poor glassy lava covering >100 km^2 of the 300 km^2 basin (Fig. 1B). Pumice and ash fall deposits associated with the explosive phase of each rhyolitic eruption are preserved in Argentina and likely are equal in volume to these lava flows (Fierstein et al., 2013). This is the greatest concentration of post-glacial rhyolite in the Andes. The only comparable Holocene rhyolite flare-up globally comprises >4 km^3

of rhyolite lava and tephra that occur along the 15 km Mono Craters chain in California (Hildreth, 2004). Building on Hildreth et al. (2010) and Singer et al. (2000), ongoing efforts to determine the ages of youngest lavas using the $^{40}Ar/^{39}Ar$ method and distal ash beds using ^{14}C indicate that silicic volcanism is concentrated in two phases separated by a 5–10 k.y. period during which eruptions were relatively small and less frequent (Andersen et al., 2013; Fierstein et al., 2013) (Fig. 2). Coincident with deglaciation, phase 1 began with the eruption of the rhyolite east of Presa Laguna del Maule (unit *rep*; Fig. 1B). Following this eruption, numerous andesitic flows and rhyodacitic domes were erupted, primarily along the western shore of the lake. Phase 1 culminated in the eruption of two high-silica rhyolite flows at 22.5 and 19 ka—respectively, the rhyolite of Arroyo Palacios (unit *rap*) and the Espejos Rhyolite (unit *rle*). Phase 2 began in the Holocene with the eruption of the earliest Barrancas complex (unit *rcb*) at the southeastern end of the lake (Figs. 1B and 2B). Rhyolitic eruptions continue into the late Holocene in the southern and eastern basin at the Cari Launa (units *rsl*, 3.5 ka, and *rcl*), Divisoria (unit *rcd*, 2.2 ka), and Nieblas (unit *rln*) eruptive centers. The eruption rate increased with time, with the phase 2 average nearly double that of phase 1 (Fig. 2C).

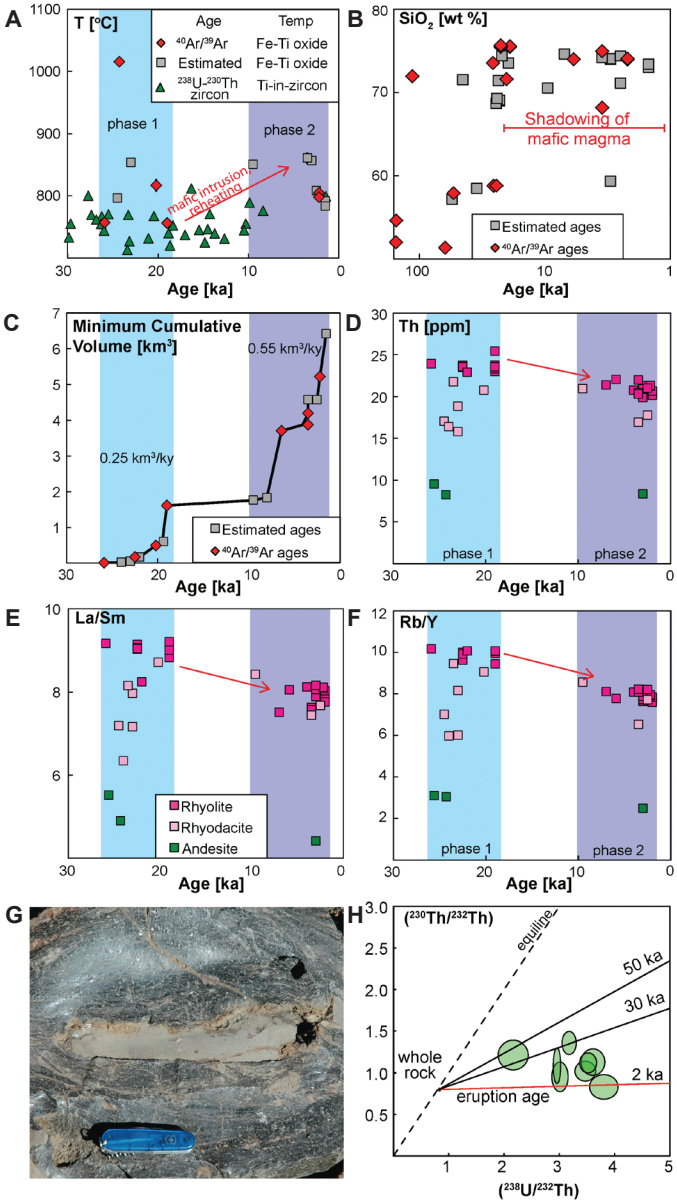

Figure 2. (A) Post-glacial variation of magma temperature. Temperatures associated with $^{40}Ar/^{39}Ar$ or estimated eruption ages are determined by two-oxide thermometry (Ghiorso and Evans, 2008) while zircon $^{238}U/^{230}Th$ ages are associated with Ti-in-zircon temperatures (Ferry and Watson, 2007). (B). SiO_2 content of Laguna del Maule lavas for the past 160 k.y.; note the different x-axis scale versus the other panels. Previously common mafic eruptions are rare and peripheral since the 19 ka Espejos eruption. (C) The cumulative volume of post-glacial silicic lava. Plotted data and rates are minimums because they do not account for tephra fall preserved in Argentina. (D–F) Trace element compositions of the post-glacial lavas display spatially independent, temporally coherent chemical evolution consistent with an integrated, relatively homogeneous source reservoir. Symbols are as listed in panel E. (G) Quenched basaltic andesite inclusion in the rhyodacite of Colada Dendriforme (*rdcd*). (H) $^{230}Th/^{238}U$ equiline plot of data from euhedral surfaces of zircon in Nieblas rhyolite pumice. The red 2 ka isochron corresponds to the estimated eruption age. Black 30 and 50 ka isochrons are for reference. Isochrons calculated using the whole-rock Nieblas rhyolite $^{238}U/^{230}Th$ composition.

Whereas there have been few mafic eruptions in the past 20 k.y., textural and chemical evidence that mafic magma has intruded to shallow depths is clear. Quenched inclusions of basaltic andesite are common in the early post-glacial rhyodacites (Fig. 2G), indicating physical interactions between hot mafic magma and cooler silicic magmas. While the rhyolite lavas are notably free of such inclusions, the 100 °C range and temporal trend in pre-eruptive magma storage temperatures are consistent with reheating of the silicic system by recent mafic intrusion (Fig. 2A). Reconnaissance measurements of soil gas have revealed emissions of CO_2 of between 0.5% and 1.0% (vol.) throughout the basin and up to 7% (vol.) along the northern lakeshore. Because the solubility of CO_2 in rhyolite is limited (e.g., Lowenstern et al., 2006), these findings suggest that the inflation may reflect intrusion of mafic magma.

Phenocrysts in large silicic ash flow tuffs reveal magma residence times up to several hundred thousand years (Costa, 2008; Reid, 2008; Simon et al., 2008; Wotzlaw et al., 2013). However, these estimates are complicated by diverse crystal populations, including autocrysts that crystallized from the erupted melt, antecrysts that may have grown from earlier melts, and xenocrysts from wallrocks (Charlier et al., 2004; Cooper and Reid, 2008). Using a sensitive high-resolution ion microprobe–reverse geometry (SHRIMP-RG) instrument and secondary ion mass spectrometry, $^{230}Th/^{238}U$ disequilibrium dates were obtained from the outer surfaces of zircons in the <2 ka Nieblas rhyolite (Andersen et al., 2013). Model ages range from ca. 2 ka to 42 ka, demonstrating

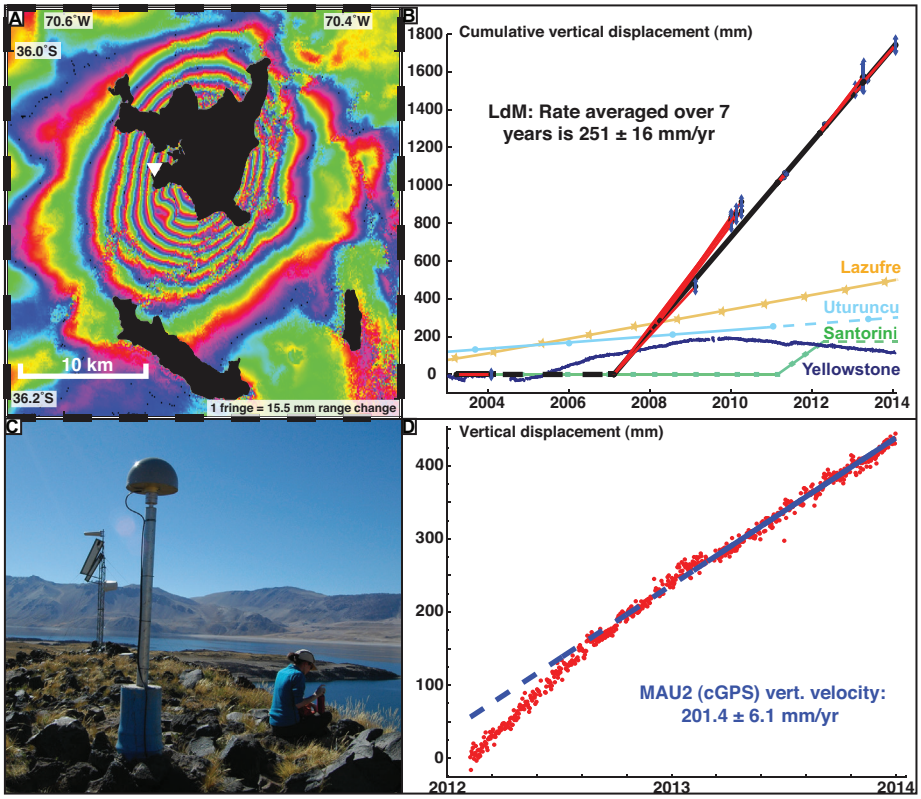

Figure 3. (A) InSAR interferogram spanning 14 Apr. 2013 to 25 Jan. 2014. One fringe denotes 15.5 mm of range change between satellite and ground. (B) Time series of vertical uplift calculated from InSAR models using ENVISAT, ALOS, and TerraSAR-X data between 2003 and 2014 (Feigl et al., 2014 [up to 2012]). Yellowstone cGPS data are shown for comparison at station WLMY (Chang et al., 2010). Other curves are estimated from GPS and InSAR results at Lazufre and Uturuncu (Pearse and Lundgren, 2013; Henderson and Pritchard, 2013) and Santorini (Newman et al., 2012; Parks et al., 2012). Dashed lines extrapolated based on personal communication with these authors. (C) View east from the MAU2 cGPS station and the most rapidly deforming area on the west side of Laguna del Maule (photo by L. Cordova, March 2012). (D) Time series between 2012 and 2014 of relative vertical displacement for cGPS station MAU2 with respect to South America and the best-fitting velocity (blue line).

zircon residence and assembly of the system over as much as 40 k.y. (Fig. 2H).

Geodetic and Geophysical Evidence of Current Processes, Unrest, and System Structure

The Laguna del Maule volcanic field is currently deforming at an exceptionally high rate. Using interferometric analysis of synthetic aperture radar (InSAR) data, Fournier et al. (2010) found the rate of surface deformation to be negligible from January 2003 to February 2004, but that inflation accelerated rapidly between 2004 and 2007. Using InSAR data acquired between 2007 and 2012, Feigl et al. (2014) found uplift rates exceeding 280 mm/yr (Fig. 3). Feigl et al. (2014) modeled the source as a 9.0 × 5.3 km inflating sill at a depth of 5.2 km, assuming a rectangular dislocation in a half space with uniform elastic properties. From January 2004 to April 2012, the total increase in volume was 0.15 km^3. The high rate of deformation is confirmed by continuous Global Positioning System (cGPS) measurements at five OVDAS stations between 2012 and 2014 (Fig. 3) (Le Mével et al., 2013; Feigl et al., 2014). During this ongoing episode of unrest, the rate of deformation at Laguna del Maule has been among the highest ever measured at a volcano that is not actively erupting. For example, the remarkable inflation episodes at Yellowstone (Chang et al., 2010) and Santorini (Newman et al., 2012) calderas occurred at rates 2–5 times slower than at Laguna del Maule (Fig. 3). Uplift at Uturuncu volcano, in the Central Andes above the vast and deep Altiplano Puna magma body, is an order of magnitude slower than at Laguna del Maule (Henderson and Pritchard, 2013; del Potro et al., 2013). The inferred rate of magma intrusion at Laguna del Maule of 0.03 km^3/kyr is twice that at Santorini (Parks et al., 2012).

The electrical resistivity of crustal rocks is sensitive to temperature, fluid content, and the degree of hydrothermal alteration (Unsworth and Rondenay, 2013). The resistivity structure around Laguna del Maule was investigated with commercial magnetotelluric (MT) surveys commissioned for geothermal exploration by Alterra Power in 2009–2011. A subset of these MT data have been used to create both 2-D and 3-D inversion models. The 3-D inversion used the algorithm of Siripunvaraporn et al. (2005), and a representative model is shown in Figure 4. It shows a zone of low resistivity under the western half of Laguna del Maule at a depth of ~5 km below the surface. This feature likely represents a magma body and an associated hydrothermal system (Fig. 4). The resistivity values of this feature are consistent with a zone of 10%–20% rhyolitic melt with the water and Na_2O concentrations determined from the recently erupted rhyolites (Pommier and Le Trong, 2011) (Fig. 2). The location agrees very well with the inflation source inferred from the geodetic data (Fig. 3).

In the area of maximum uplift along the southwestern shores of Laguna del Maule, 30-m-thick outcrops of Late Pleistocene diatomaceous lacustrine sediments are weakly tilted, cut by numerous normal faults with centimeters of offset, and may reflect long-term uplift over decades (Hildreth et al., 2010; Andersen et al., 2013). These observations are consistent with the radial pattern of deformation observed geodetically.

Of 223 located earthquakes in the vicinity of Laguna del Maule recorded by the five OVDAS seismometers between April 2011 and January 2014, 154 (69%) are shallower than 5 km, and 91% of these had a local magnitude ≤2, with most occurring beneath the recent Nieblas (*rln*) and Barrancas (*rcb*) rhyolite vents, along the periphery of the uplifting region (Fig. 5). Both

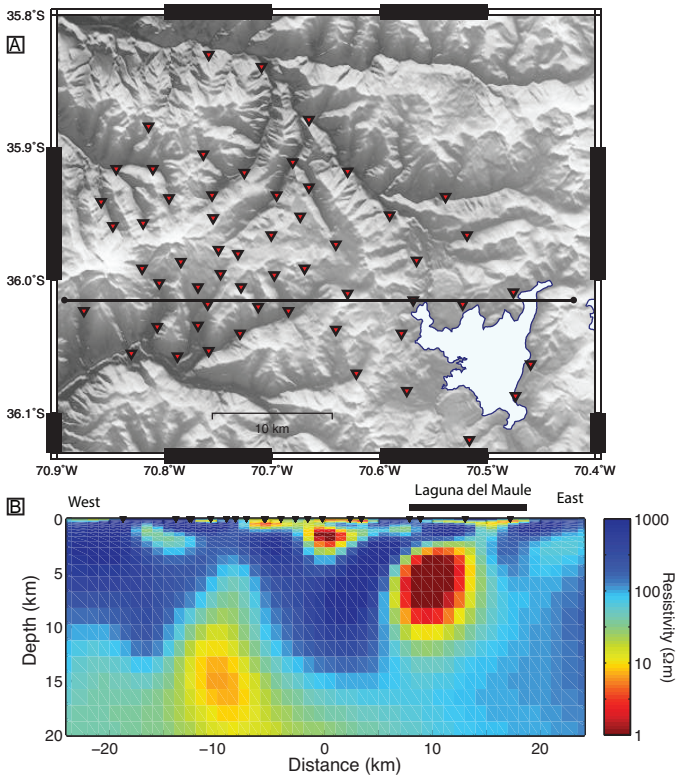

Figure 4. (A) Locations of 56 broadband magnetotelluric (MT) stations measured during a geothermal study by Alterra Power. (B) An east-west slice of a 3-D electrical resistivity model obtained by inversion of these MT data. Location of slice shown in (A). MT data were inverted in frequency band 100–0.01 Hz and have a statistically acceptable root-mean-square fit of 1.8.

short-period volcano-tectonic (VT) and long-period earthquakes are concentrated in these zones. On 11–12 January 2013 OVDAS recorded a swarm of 240 VT earthquakes of M ≤1.3 located ~9 km SW of the lake at depths shallower than 5 km (Fig. 5). This earthquake swarm may have resulted from pressurization of fluids and faults distal to an intruding body of magma (e.g., Manga and Brodsky, 2006).

To evaluate the mass changes at depth—and constrain the contribution of fluids and/or magma to the uplift signal—we are also conducting a dynamic gravity study in order to evaluate temporal changes. Using three gravimeters, a network of 37 stations (Fig. 1B) was installed in April 2013 and re-occupied in January 2014. Preliminary results suggest widespread positive residual gravity changes (>30 μGal) throughout the lake basin during the ten months between occupations. A −10 mGal gravity low exists along the western margin of the lake, as delineated by the reconnaissance study of Honores (2013). Our dynamic gravity network will also expand this Bouguer survey to help delineate the magma body below the lake.

CURRENT HYPOTHESES, CONCLUSIONS, AND FUTURE WORK

The "magmatic mush" model of Hildreth (2004) and Hildreth and Wilson (2007) was developed to explain volcanological, petrological, and structural observations of the Long Valley magma system from which the compositionally and thermally zoned crystal-poor rhyolite of the 650 km^3 Bishop Tuff erupted at 767 ka. In this model, the magma system comprises a relatively thin boundary layer of granitoid that solidified against the country rocks, inboard of which is a rigid "sponge" of mainly crystals with minor interstitial melt. Within this rigid zone is an extensive reservoir of crystal-rich mush that is maintained in a partially molten state via fluxing of heat and mafic magma through the basal parts of the crustal reservoir. The amalgamation of melt-rich lenses near the roof creates a low-density barrier that blocks the ascent of mafic magma to the surface (Hildreth, 2004). The crystal-poor, melt-dominated zone near the roof of such a system is a magma chamber that may be tapped to feed rhyolitic eruptions.

Our observations—including the basin-wide, temporally correlated, chemical evolution; the distribution of silicic vents ringing the lake basin during the past 25 k.y. (Fig. 1B); the juxtaposition of peripheral mafic and bimodal eruptions with the central ring of rhyolites that are devoid of mafic inclusions; the high rate of surface deformation; MT evidence of a large body of fluid at a depth of 5 km; the concentration of shallow earthquakes; zircon phenocrysts that record ~40 k.y. of magma residence; and changes in gravity—collectively support the working hypothesis in Figure 6. We propose that the silicic vents have tapped crystal-poor, rhyolitic melt that segregated from an extensive crystal-rich mush zone that had become established beneath much of the basin by ca. 20 ka, as indicated by eruption of units *rle, rap, rdac*, and *ras* (Fig. 1B). Crystal-poor melt later fueled the Holocene rhyolite eruption of units *rsl, rcl, rcd, rng, rcb*, and *rln*. What remains unclear is whether a crystal-poor rhyolitic melt layer that intercepts mafic recharge magma at deep levels currently caps the entire magmatic system or, alternatively, if the current unrest reflects a singular intrusive event rebuilding toward such a configuration.

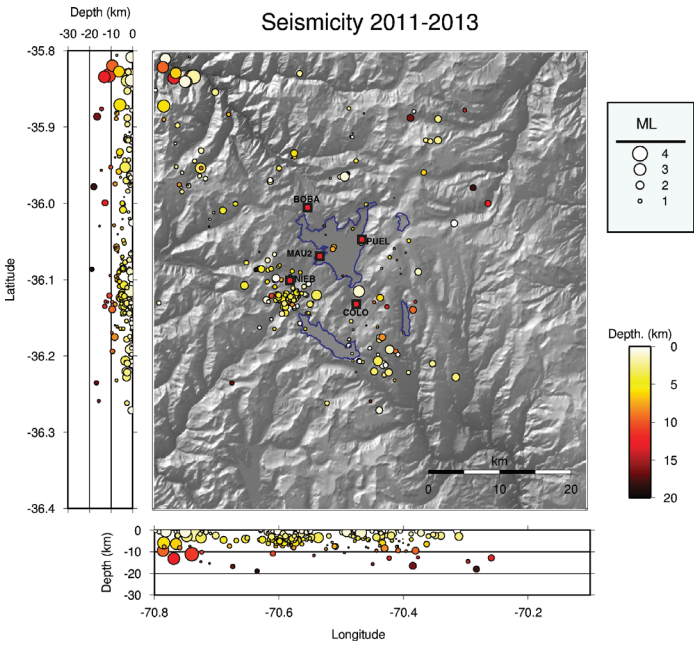

Figure 5. Located earthquakes recorded by OVDAS network of five seismic stations (red squares: BOBA, COLO, MAU2, NIEB, and PUEL) from April 2011 to January 2014.

The model of Jellinek and DePaolo (2003) relates magma supply, wallrock viscosity, and the volume of eruptible magma in a chamber. For the Laguna del Maule system, we estimate a recurrence interval of one dike-fed eruption every ~1000 years to generate the 24 silicic vents and take this as the elastic pressurization time t_e. Constraints on the long-term magma supply rate, Q, are as follows: The minimum value of Q of 0.0005 km^3/yr assumes an eruptive volume of 13 km^3 of silicic magma over the past 25 k.y. that includes an estimate of tephra volume equal to that of the lavas (Fierstein et al., 2013). The maximum value of Q of 0.03 km^3/yr is based on the model of an inflating sill needed to drive the ongoing deformation by Feigl et al. (2014). These parameters suggest that the magma body (melt + mush) supplying rhyolite into dikes that have erupted has a volume of at least 100 km^3 and more likely several hundred cubic kilometers (see figure 6 *in* Jellinek and DePaolo, 2003). As the magma body takes on a flattened, disc-shaped form via lateral spreading, hoop stresses concentrate at the intrusion's edges, allowing dikes to form around its periphery—consistent with the spatial distribution of vents at Laguna del Maule (Jellinek and DePaolo, 2003).

Testing the hypothesis outlined in Figure 6 using a variety of geophysical, geochemical, and computational approaches is now an important goal of our team, and it is highlighted at http://geoscience.wisc.edu/rhyolitic/. For example, using an array of temporary seismometers to augment the OVDAS network, passive source seismology can provide both (a) a synoptic image of the seismic structure of the crust, and (b) evidence for temporal change in the magmatic system. The electrical resistivity survey by Alterra Power was planned to image the geothermal system northwest of Laguna del Maule. These data clearly detect the low resistivity body beneath the lake (Fig. 4) that is likely an accumulation of melt. However, the station spacing is insufficient to define the geometry of this magma body. A dense array of MT stations within the basin would allow the 3-D geometry of the magma body to be better defined and give more robust estimates of the resistivity that can lead to improved constraints on the quantity and composition of magma. Similarly, as station density is increased, further changes in the gravity field may be detected at a spatial resolution that can resolve fluid/magma pathways, the geometry of the magma reservoir, and whether the source responsible for the uplift is intruding magma or lower density hydrothermal fluid. Continuing the InSAR and GPS measurements will ensure that changes in seismicity or the gravity field are measured coevally with the deformation. Studies of trace element zoning in phenocrysts in the rhyolites are under way, in parallel with expanded ^{230}Th/^{238}U dating of zircons, to constrain the number, extent, and timing of mixing events between mafic and silicic magmas, and the longevity of the silicic reservoir. Quantifying the flux and isotopic composition of diffuse CO_2 would help gauge the addition of any basaltic magma. Mapping of fault displacements in the uplifted lacustrine sediments may help quantify long-term deformation rates. These sets of geophysical and geochemical observations will be used in numerical models at a variety of scales, including micro- and meso-scale magma chamber simulations linked directly to a macro-scale finite element model of crustal deformation. The aim is to create a unified model of magmatic system dynamics using Laguna del Maule as the example.

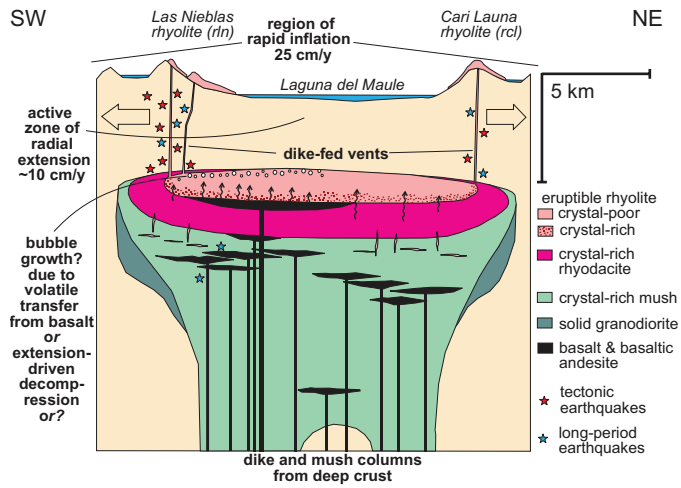

Figure 6. Hypothesized magmatic system feeding the crystal-poor rhyolitic eruptions encircling Laguna del Maule (adapted from Hildreth, 2004). Section is SW-NE along bent line in Figure 1B. Observations support inferences shown here, including: (1) rapid uplift, (2) shallow earthquakes, (3) active intrusion of mafic magma at 5 km depth, and (4) normal faulting and geodetic data that record extension.

ACKNOWLEDGMENTS

Hildreth and Fierstein were supported by the U.S. Geological Survey and Servicio Nacional de Geología y Minería of Chile, leading to the map on which Fig. 1B is based and the eruptive history in Boletin 63. Support includes NSF RAPID grant EAR-1322595, NASA grant NNX12AO37G, a student research grant from the Geological Society of America, and Canadian NSERC Discovery and Mitacs-Accelerate grants. The 3-D MT inversion was performed on the high performance cluster developed by Compute Canada/Westgrid using an algorithm provided by Weerachai Siripunvaraporn. We thank Catherine Hickson and Alterra Power for sharing MT data. The "Alcalde del Mar," don Luis Torres, is thanked for hospitality and assistance in safely navigating the windswept Laguna. We are grateful for assistance from Neal Lord, Tor Stetson-Lee, Erin Birsic, Nico Garibaldi, Meagan Ankney, Brian Beard, Clark Johnson, and Marsha Lidzbarski. Comments by Calvin Miller and two anonymous reviewers improved the manuscript.

REFERENCES CITED

Andersen, N.L., Singer, B.S., Jicha, B.R., Fierstein, J., and Vazquez, J.A., 2013, The development of a restless rhyolite magma chamber at Laguna del Maule, Chile: American Geophysical Union Fall Meeting abstract V51C–2676.

Bachmann, O., and Bergantz, G.W., 2008, Rhyolites and their source mushes across tectonic settings: Journal of Petrology, v. 49, p. 2277–2285, doi: 10.1093/petrology/egn068.

Battaglia, M., Segall, P., and Roberts, C., 2003, The mechanics of unrest at Long Valley Caldera, California. 2. Constraining the nature of the source using geodetic and micro-gravity data: Journal of Volcanology and Geothermal Research, v. 127, no. 3–4, p. 219–245, doi: 10.1016/S0377-0273(03)00171-9.

Chang, W.L., Smith, R.B., Farrell, J., and Puskas, C.M., 2010, An extraordinary episode of Yellowstone caldera uplift, 2004–2010, from GPS and InSAR observations: Geophysical Research Letters, v. 37, L23302, doi: 10.1029/2010GL045451.

Charlier, B.L.A., Wilson, C.J.N., Lowenstern, J.B., Blake, S., Van Calsteren, P.W., and Davidson, J.P., 2004, Magma generation at a large, hyperactive silicic volcano (Taupo, New Zealand) revealed by U-Th and U-Pb systematics in zircons: Journal of Petrology, v. 46, p. 3–32, doi: 10.1093/petrology/egh060.

Cooper, K.M., and Reid, M.R., 2008, Uranium-series crystal ages: Reviews in Mineralogy and Geochemistry, v. 69, p. 479–544, doi: 10.2138/rmg.2008.69.13.

Costa, F., 2008, Residence times of silicic magmas associated with calderas: Developments in Volcanology, v. 10, p. 1–55, doi: 10.1016/S1871-644X(07)00001-0.

del Potro, R., Díez, M., Blundy, J., Gottsmann, J., and Camacho, A., 2013, Diapiric ascent of silicic magma beneath the Bolivian Altiplano: Geophysical Research Letters, v. 40, p. 2044–2048, doi: 10.1002/grl.50493.

Farrell, J., Smith, R.B., Husen, S., and Diehl, T., 2014, Tomography from twenty-six years of seismicity reveals the spatial extent of the Yellowstone crustal magma reservoir extends well beyond the Yellowstone caldera: Geophysical Research Letters, v. 41, doi: 10.1002/2014GL059588.

Feigl, K.L., Le Mével, H., Ali, S.T., Cordova, L., Andersen, N.L., DeMets, C., and Singer, B.S., 2014, Rapid uplift in Laguna del Maule volcanic field of the Andean Southern Volcanic Zone (Chile) 2007–2012: Geophysical Journal International, v. 196, p. 885–901, doi: 10.1093/gji/ggt438.

Ferry, J.M., and Watson, E.B., 2007, New thermodynamic models and revised calibrations for the Ti-in-zircon and Zr-in-rutile thermometers: Contributions to Mineralogy and Petrology, v. 154, p. 429–437, doi: 10.1007/s00410-007-0201-0.

Fierstein, J., Sruoga, P., Amigo, A., Elissondo., M., and Rosas, M., 2013, Tephra in Argentina establishes postglacial eruptive history of Laguna del Maule volcanic field in Chile: IAVCEI 2013 Scientific Assembly abstract 3A2_3F–O11, 23 July.

Fournier, T.J., Pritchard, M.E., and Riddick, S.N., 2010, Duration, magnitude, and frequency of subaerial volcano deformation events: New results from Latin America using InSAR and global synthesis: Geochemistry Geophysics Geosystems, v. 11, doi: 10.1029/2009GC002558.

Ghiorso, M.S., and Evans, B.W., 2008, Thermodynamics of rhombohedral solid solutions and a revision of the Fe-Ti two-oxide geothermometer and oxygen-barometer: American Journal of Science, v. 308, p. 957–1039, doi: 10.2475/09.2008.01.

Henderson, S.T., and Pritchard, M.E., 2013, Decadal volcanic deformation of the Central Andes Volcanic Zone revealed by InSAR time series: Geochemistry Geophysics Geosystems, v. 14, p. 1358–1374, doi: 10.1002/ggge.20074.

Hildreth, W., 2004, Volcanological perspectives on Long Valley, Mammoth Mountain, and Mono Craters: Several contiguous but discrete systems: Journal of Volcanology and Geothermal Research, v. 136, p. 169–198, doi: 10.1016/j.jvolgeores.2004.05.019.

Hildreth, W., and Wilson, C.J.N., 2007, Compositional zoning of the Bishop Tuff: Journal of Petrology, v. 48, p. 951–999, doi: 10.1093/petrology/egm007.

Hildreth, W., Godoy, E., Fierstein, J., and Singer, B., 2010, Laguna del Maule Volcanic Field: Eruptive history of a Quaternary basalt-rhyolite distributed vent volcanic field on the Andean rangecrest in central Chile: Santiago, Chile, Servicio Nacional de Geología y Minería, Boletin v. 63, 145 p.

Honores, C.C., 2013, Estudio del la deformación de la caldera Laguna del Maule [M.Sc. thesis]: Universidad de Chile, Santiago, Chile, Facultad de Ciencias Físicas y Matemáticas, Departamento de Geofísica, 79 p.

Jellinek, A.M., and DePaolo, D.J., 2003, A model for the origin of large silicic magma chambers: Precursors of caldera-forming eruptions: Bulletin of Volcanology, v. 65, p. 363–381, doi: 10.1007/s00445-003-0277-y.

Le Mével, H., Cordova, L., Ali, S.T., Feigl, K.L., DeMets, C., Williams-Jones, G., Tikoff, B., and Singer, B.S., 2013, Unrest within a large rhyolitic magma system at Laguna del Maule volcanic field (Chile) from 2007 through 2013: Geodetic measurements and numerical models: AGU Fall Meeting Abstracts, v. 1, p. 2728.

Lowenstern, J.B., Smith, R.B., and Hill, D.P., 2006, Monitoring super-volcanoes: Geophysical and geochemical signals at Yellowstone and other large caldera systems: Philosophical Transactions of the Royal Society of London Series A-Mathematical Physical and Engineering Sciences, v. 364, p. 2055–2072.

Manga, M., and Brodsky, E., 2006, Seismic triggering of eruptions in the far field: Volcanoes and geysers: Annual Review of Earth and Planetary Sciences, v. 34, p. 263–291, doi: 10.1146/annurev.earth.34.031405.125125.

Newman, A.V., Stiros, S., Feng, L.J., Psimoulis, P., Moschas, F., Saltogianni, V., Jiang, Y., Papazchos, C., Panagiotopoulos, D., Karagianni, E., and Vamcakaris, D., 2012, Recent geodetic unrest at Santorini Caldera, Greece: Geophysical Research Letters, v. 39, doi: 10.1029/2012GL051286.

Parks, M.M., Biggs, J., England, P., Mather, T.A., Nomikou, P., Palamartchouk, K., Papanikoalaou, X., Paradissis, D., Parsons, B., Pyle, D.M., Raptakis, C., and Zacharis, V., 2012, Evolution of Santorini volcano dominated by episodic and rapid fluxes of melt from depth: Nature Geoscience, v. 5, p. 749–754, doi: 10.1038/ngeo1562.

Pearse, J., and Lundgren, P., 2013, Source model of deformation at Lazufre volcanic center, central Andes, constrained by InSAR time series: Geophysical Research Letters, v. 40, p. 1059–1064, doi: 10.1002/grl.50276.

Pommier, A., and Le Trong, E., 2011, SIGMELTS: A web portal for electrical conductivity calculations in geosciences: Computers & Geosciences, v. 37, p. 1450–1459, doi: 10.1016/j.cageo.2011.01.002.

Reid, M.R., 2008, How long does it take to supersize an eruption?: Elements, v. 4, p. 23–28, doi: 10.2113/GSELEMENTS.4.1.23.

Romero, A.E., McEvilly, T.V., Majer, E.L., and Michelini, A., 1993, Velocity structure of the Long Valley caldera from the inversion of local earthquake P-travel and S-travel times: Journal of Geophysical Research, v. 98, p. 19,869–19,879, doi: 10.1029/93JB01553.

Self, S., 2006, The effects and consequences of very large explosive volcanic eruptions: Philosophical Transactions of the Royal Society of London. Series A, Mathematical and Physical Sciences, v. 364, p. 2073–2097.

Self, S., and Blake, S., 2008, Consequences of explosive supereruptions: Elements, v. 4, p. 41–46, doi: 10.2113/GSELEMENTS.4.1.41.

Simon, J.I., Renne, P.R., and Mundil, R., 2008, Implications of pre-eruptive magmatic histories of zircons for U-Pb geochronology of silicic extrusions: Earth and Planetary Science Letters, v. 266, p. 182–194, doi: 10.1016/j.epsl.2007.11.014.

Singer, B., Hildreth, W., and Vinzce, Y., 2000, $^{40}Ar/^{39}Ar$ evidence for early deglaciation of the central Chilean Andes: Geophysical Research Letters, v. 27, p. 1663–1666, doi: 10.1029/1999GL011065.

Siripunvaraporn, W., Egbert, G.D., Lenbury, Y., and Uyeshima, M., 2005, Three-dimensional magnetotelluric inversion: Data subspace method: Physics of the Earth and Planetary Interiors, v. 150, p. 3–14, doi: 10.1016/j.pepi.2004.08.023.

Sparks, S.J., Self, S., Grattan, J., Oppenheimer, C., Pyle, D., and Rymer, H., 2005, Super-eruptions: Global effects and future threats: Report of a Geological Society of London Working Group: London, The Geological Society, 24 p.

Steck, L.K., Thurber, C.H., Fehler, M.C., Lutter, W.J., Roberts, P.M., Baldridge, W.S., Stafford, D.G., and Sessions, R., 1998, Crust and upper mantle P wave velocity structure beneath Valles caldera, New Mexico: Results from the Jemez teleseismic tomography experiment: Journal of Geophysical Research–Solid Earth, v. 103, p. 24,301–24,320, doi: 10.1029/98JB00750.

Tizzani, P., Battaglia, M., Zeni, G., Atzori, S., Berardino, P., and Lanari, R., 2009, Uplift and magma intrusion at Long Valley Caldera from InSAR and gravity measurements: Geology, v. 37, p. 63–66, doi: 10.1130/G25318A.1.

Unsworth, M.J., and Rondenay, S., 2013, Mapping the distribution of fluids in the crust and lithospheric mantle utilizing geophysical methods, *in* Harlov, D.E., and Austrheim, H., eds., Metasomatism and the Chemical Transformation of Rock: The Role of Fluids in Crustal and Upper Mantle Processes Series, Lecture Notes in Earth System Sciences, Berlin, Springer-Verlag, p. 535–598, doi: 10.1007/978-3-642-28394-9_13.

Wilson, C.J.N., 2008, Supereruptions and supervolcanoes: Processes and products: Elements, v. 4, p. 29–34, doi: 10.2113/GSELEMENTS.4.1.29.

Wilson, C.J.N., Blake, S., Charlier, B.L.A., and Sutton, A.N., 2005, The 26.5 ka Oruanui Eruption, Taupo Volcano, New Zealand: Development, characteristics, and evacuation of a large rhyolitic magma body: Journal of Petrology, v. 47, p. 35–69, doi: 10.1093/petrology/egi066.

Wotzlaw, J.-F., Schaltegger, U., Frick, D.A., Dungan, M.A., Gerdes, A., and Gunther, D., 2013, Tracking the evolution of large-volume silicic magma reservoirs from assembly to supereruption: Geology, v. 41, p. 867–870, doi: 10.1130/G34366.1.

Manuscript received 12 Mar. 2014; accepted 5 June 2014. ❇